First-Principles Study of Bipolar Dopability in the $CuInO_2$ Transparent Semiconductor

Li Liu,[†,‡] Kewu Bai,[†] Hao Gong,[‡] and Ping Wu*[,†]

Institute of High Performance Computing, 1 Science Park Road, #01-01 The Capricorn, Singapore 117528, and Department of Materials Science, National University of Singapore, 10 Kent Ridge Crescent, Singapore 119260

Received May 17, 2005. Revised Manuscript Received August 25, 2005

In this study, we explored the fundamental problem of defect formation in $CuInO_2$ through first-principles DFT calculations. All kinds of point defects were first examined in their neutral states, and then several defects with relatively low formation energy at neutral state were studied in all possible charge states. As a first systematic point defect study on $CuInO_2$, our work found that the p-type intrinsic point defects are more abundant and the defect levels are shallower than the n-type ones. There is hence asymmetry of p- vs n-type in terms of intrinsic doping. Our study not only enhanced the understanding of the fundamental electronic structures of $CuInO_2$ but also provided practical guidance to the development of $CuInO_2$-based devices.

1. Introduction

Transparent conductive oxides (TCOs) have band gaps above 3 eV and, typically, may be doped for either n- or p-type conduction, but not both. Different explanations[1] were proposed for this difficulty in bidoping. Among them was the compensation effect caused by intrinsic point defects. According to the explanations, a wide band gap could promote the formation of compensating intrinsic point defects that always act to negate the effect of doping.[2] In general, a wide band gap semiconductor would tend to be n-type if the dominant intrinsic point defects introduce full states near the conduction band minimum (CBM) and be p-type if the dominant defects introduce empty electronic states near the valence band maximum (VBM). Therefore, defect formation mechanisms are of fundamental importance in the understanding and design of new wide band gap semiconductors.

Some delafossite TCOs, like $CuAlO_2$ and $CuGaO_2$, are intrinsically semiconducting without intentional doping. Thus, it may be of great interest to study the intrinsic point defects of this group of materials to understand their properties. However, to the best of our knowledge, little modeling work has been reported.

Experimenters have their hands tied in defect physics studies due to the difficulty of detecting defects of trace amount or of small atomic number, both of which could be true in the defect study of delafossite oxides. With a neat packing of hexagonal net layers of homoatoms, delafossites are not expected to accommodate a large amount of defects. This is true especially for $CuAlO_2$ and $CuFeO_2$ when a small trivalent cation occupies the center of the oxygen octahedral. In the case of $CuInO_2$, however, it was found that the structure could hold extra oxygen atoms in the lattice.[3] Even so, intrinsic defects other than extra oxygen are not reported hitherto.

A theoretical method is of special priority in the study of defect physics due to its superiority in control. However, only two reports on the theoretical study of defect physics for the delafossite family are available, despite the mysterious p-type conductivity in the stoichiometric $CuAlO_2$, a prototype of delafossite TCO. Katayama-Yoshida et al.[4] studied the formation energy and impurity levels of cation vacancies and selective dopant (Be^{2+}, Mg^{2+}, and Ca^{2+}) substitutes in $CuAlO_2$ within the local density approximation (LDA). Their calculation results suggesting copper vacancy (V_{Cu}) and Be dopant at the Al site (Be_{Al}) with lower impurity levels are promising point defects for higher p-type conductivity. However, the supercell employed in their study contained only 32 atoms, which is probably insufficient to avoid artificial interaction between defects, on the basis of our supercell size convergence test. The other theoretical report on the defect physics of this group of compounds was given by Nie et al.[5] They calculated the formation energy for some typical intrinsic defects (two vacancies, V_{Cu} and V_O, and one interstitial Cu_i) in $CuGaO_2$. Comparing with their previous

* Corresponding author. Phone: 65-6419-1212. Fax: 65-6778-0522. E-mail: wuping@ihpc.a-star.edu.sg.
† Institute of High Performance Computing.
‡ National University of Singapore.

(1) Zhang, S. B.; Wei, S.-H.; Zunger, A. *Physica B* **1999**, *273*−*274*, 976. Laks, D. B.; Van de Walle, C. G.; Neumark, G. F.; et al. *Phys. Rev. B* **1992**, *45*, 10965. Chadi, D. J.; Chang, K. J. *Appl. Phys. Lett.* **1989**, *55*, 575. Jenkins, D. W.; Dow, J. D. *Phys. Rev. B* **1989**, *39*, 3317. Neumark, G. F. *Phys. Rev. Lett.* **1989**, *62*, 1800. Ren, S. Y.; Dow, J. D.; Klemm, S. *J. Appl. Phys.* **1989**, 66, 2065. Mandel, G. *Phys.* Rev. **1964**, *134*, A1073.

(2) Zhang, S. B. *J. Phys.: Condens. Matter* **2002**, *14*, R881. Zhang, S. B.; Wei, S.-H.; Zunger, A. *Phys. Rev. Lett.* **2000**, *84*, 1232. Walukiewicz, W. In *Defects in Optoelectronic Materials*; Wada, K., Pang, S., Ed.; C&B Science Publishers: New York, 1999. Ferreira, S. O.; Sitter, H.; Faschinger, W.; et al. *J. Cryst. Growth* **1995**, *146*, 418.

(3) Park, S.; Keszler, D. A. *J. Solid State Chem.* **2003**, *173*, 355.

(4) Katayama-Yoshida, H.; Koyanagi, T.; Funashima, H.; et al. *Solid State Commun.* **2003**, *126*, 135.

(5) Nie, X. L.; Wei, S.-H.; Zhang, S. B. *Phys. Rev. Lett.* **2002**, *88*, 066405.

10.1021/cm051048k CCC: $30.25
Published on Web 10/04/2005

point defect calculations on ZnO, they found that the formation of defects that are expected to be shallow acceptors is much easier than that in ZnO, while the formation of the compensating defects (or donor-like defects, like V_O and Cu_i) is harder for $CuGaO_2$. They thus extrapolated that a great reduction in self-compensation and lower acceptor formation energy signal p-type conductivity in $CuM^{III}O_2$ compounds. However, almost no calculation details or concrete data on formation energy or defect levels were provided in Nie's publication.[5]

A lack of systematic study on the defect physics of this group of material, possibly due to the complexity of the problem for a ternary compound compared with ZnO, will certainly hinder our comprehension on the underlying mechanism of their unusual p-type electrical conductivity. Moreover, despite the improved experimental work on $CuInO_2$,[3,6−9] few theoretical studies have been carried out on this material, even compared with $CuAlO_2$. Therefore, our work aims to fill this void. In this paper, a systematic theoretical study on the isolated defects in $CuInO_2$ is given with all intrinsic point defects being carefully examined. Our goal is to identify the intrinsic point defect and to examine the bipolar dopability in $CuInO_2$ with first-principles theory.

The remainder of this paper is organized as follows. In section 2, the methodology for point defect study in the first-principles scheme is briefly introduced. As the structural parameters of the conventional cell and the electronic band structure and DOS of $CuInO_2$ are the cornerstone of the defect study, their calculations are shown in section 3. Section 3 also presents the results of our calculation on the intrinsic point defects, both neutral and charged, based on the formalism in section 2. Further discussions on miscellaneous respects are presented in section 4.

2. Methodology

In this section, the first-principles approaches toward point defect study of $CuInO_2$ are presented first. Special attention is given to the determination of the chemical potential ranges of the three components. Calculation details are then summarized.

2.1. Defect Formation Energy and Defect Levels.[10,11] For a neutral defect in $CuInO_2$, the formation energy [$\Delta H_f(\alpha)$] depends on the chemical potential (μ) of each component (see section 2.2) relative to the standard value μ^0

$$\Delta H_f(\alpha,q=0) = \Delta E(\alpha,q=0) + n_{Cu}\mu_{Cu} + n_{In}\mu_{In} + n_O\mu_O \quad (1)$$

and

$$\Delta E(\alpha,q=0) = E(\alpha,q=0) - E_0(CuInO_2) + n_{Cu}\mu_{Cu}{}^0 + n_{In}\mu_{In}{}^0 + n_O\mu_O{}^0 \quad (2)$$

where $E(\alpha,q=0)$ is the total energy of the supercell containing the neutral defect α. $E_0(CuInO_2)$ is the total energy of the same supercell free of any defect. n_{Cu}, n_{In}, and n_O are the number of atoms transferred, with the subscript denoting the element. n_{Cu}, n_{In}, and n_O are positive if the atoms are transferred away from the cell and vice versa. $\mu_{Cu}{}^0$, $\mu_{In}{}^0$, and $\mu_O{}^0$ are the standard chemical potentials of the three components or the atomic total energies of the ground-state Cu (fcc), In (tetragonal), and O (α-oxygen).

A negatively charged defect can be obtained by adding an electron to the defect from the electron reservoir (Fermi level at 0 K) and vice versa. To obtain the formation energy of a charged defect, total energy was calculated with four cells: a supercell with a charged defect $\alpha[q]$ of the total energy $E^{M-q}(\alpha,q)$, a defect supercell without introducing extra charges [$E^M(\alpha,q=0)$], a perfect supercell without introducing defects or extra charge [$E^N(CuInO_2)$], and a supercell free from defects but with one component atom charged to $-q$[$E^{N+q}(CuInO_2,-q)$]. In a supercell calculation, $\Delta H_f(\alpha,q)$ is given by

$$\Delta H_f(\alpha,q) = \Delta E(\alpha,q) + n_{Cu}\mu_{Cu} + n_{In}\mu_{In} + n_O\mu_O + qE_F \quad (3)$$

with

$$\Delta E(\alpha,q) = \Delta E(\alpha,q=0) + \delta E(\alpha,q) + \delta E(CuInO_2,-q) \quad (4)$$

The first term on the right-hand side of eq 4 is given in eq 1, and the second term is as follows

$$\delta E(\alpha,q) = E^{M-q}(\alpha,q) - E^M(\alpha,q=0)$$

where $E^M(\alpha,q=0)$ is the same term as $E(\alpha,q=0)$.

The third term is given as

$$\delta E(CuInO_2,-q) = E^{N+q}(CuInO_2,-q) - E^N(CuInO_2)$$

which is the difference between the reference energy level of the defect-free $CuInO_2$ given by one-particle eigenvalue ϵ_i (e.g. i = VBM or CBM) and the energy level determined from the total-energy calculation. $\delta E(CuInO_2,-q)$ has to be considered[12] for a semiconductor with d character at the VBM, like $CuInO_2$ (as found from its PDOS in section 3). Moreover, to keep the reference eigenvalue ϵ_i in the calculation constant with or without the existence of defects, all the calculations were performed on a supercell of the same size, with the same k point sampling and by lining up the core-levels of the atoms far away from the defect in the defect cell with those in the defect-free cell accordingly.

The defect transition level $\epsilon_\alpha(q/q')$ is defined as the value of the Fermi energy (E_F) at which the formation energy of

(6) Teplin, C. W.; Kaydanova, T.; Young, D. L.; et al. *Appl. Phys. Lett.* **2004**, *85*, 3789.
(7) Sasaki, M.; Shimode, M. *J. Phys. Chem. Solids* **2003**, *64*, 1675.
(8) Garlea, O.; Bordet, P.; Darie, C.; et al. *J. Phys.: Condens. Matter* **2004**, *16*, S811. Ohta, H.; Nomura, K.; Hiramatsu, H.; et al. *Solid-State Electron.* **2003**, *47*, 2261. Ginley, D.; Roy, B.; Ode, A.; et al. *Thin Solid Films* **2003**, *445*, 193. Yanagi, H.; Ueda, K.; Ohta, H.; et al. *Solid State Commun.* **2002**, *121*, 15. Hosono, H.; Ohta, H.; Orita, M.; et al. *Vacuum* **2002**, *66*, 419. Yanagi, H.; Hase, T.; Ibuki, S.; et al. *Appl. Phys. Lett.* **2001**, *78*, 1583.
(9) Shimode, M.; Sasaki, M.; Mukaida, K. *J. Solid State Chem.* **2000**, *151*, 16.
(10) Foster, A. S.; Sulimov, V. B.; Lopez Gejo, F.; et al. *Phys. Rev. B* **2001**, *64*, 224108. Kohan, A. F.; Zhang, S. B.; Northrup, J. E. *Phys. Rev. Lett.* **1991**, *67*, 2339. Baraff, G. A.; Schluter, M. *Phys. Rev. Lett.* **1985**, *55*, 1327.
(11) Ceder, G.; Morgan, D.; Van de Walle, C. G. *Phys. Rev. B* **2000**, *61*, 15019.
(12) Zhang, S. B.; Wei, S.-H.; Zunger, A. *J. Appl. Phys.* **1998**, *83*, 3192.

defect α and charge q is equal to that of another charge state q' of the same defect, that is

$$\epsilon_\alpha(q/q') = [\Delta E(\alpha,q) - \Delta E(\alpha,q')]/(q' - q) \quad (5)$$

2.2. Limits on Atomic Chemical Potential. Chemical potentials determine the off-stoichiometry of the system and depend on different parameters, such as partial pressure and growth conditions. In a compound solid, defect properties depend on the chemical potential of the component element, as shown in eqs 1 and 3. Thermodynamic limits constrain the chemical potential values in a certain range through two criteria: first, a stable $CuInO_2$ compound has to be maintained; second, precipitation of solid elemental Cu, In, or O or end-point binary compounds should be avoided. They can be expressed mathematically as follows

$$\Delta H_f(CuInO_2) = \mu_{Cu} + \mu_{In} + 2\mu_O \quad (6)$$

$$\mu_{Cu} \le 0, \mu_{In} \le 0, \text{ and } \mu_O \le 0$$

$$2\mu_{Cu} + \mu_O \le \Delta H_f(Cu_2O) \text{ and } 2\mu_{In} + 3\mu_O \le \Delta H_f(In_2O_3) \quad (7)$$

where $\Delta H_f(CuInO_2)$, $\Delta H_f(Cu_2O)$, and $\Delta H_f(In_2O_3)$ are the calculated formation energy of $CuInO_2$, Cu_2O, and In_2O_3.

The calculated formation energies of Cu_2O, In_2O_3, and $CuInO_2$ are −1.337, −8.193, and −4.737 eV, respectively. If substituting $\Delta H_f(Cu_2O)$ and $\Delta H_f(In_2O_3)$ in eq 6 with the above values, we may have

$$\mu_{Cu} + \mu_{In} + 2\mu_O \le -4.765$$

which seems to contradict eq 6. However, if the calculation uncertainty is taken into account, this may indicate that $CuInO_2$ is metastable. Therefore, we propose to degenerate the constraints listed in eqs 6 and 7 to

$$2\mu_{Cu} + \mu_O = \Delta H_f(Cu_2O)$$

$$2\mu_{In} + 3\mu_O = \Delta H_f(In_2O_3)$$

Hence, the chemical potential ranges of the three components can be determined: $-1.34 \le \mu_O \le 0$, $-0.67 \le \mu_{Cu} \le 0$, and $-4.10 \le \mu_{In} \le -2.09$.

3. Calculation Details and Results

3.1. Calculation Details. All the calculations were performed using the plane wave basis Vienna ab initio Simulation Package (VASP) code,[13] implementing spin-polarized periodic density functional calculations (DFT) and generalized gradient approximation (GGA).[14] The interaction between the core and valence-electrons is described using the ultrasoft pseudopotentials (USPP) introduced by Vanderbilt[15] and provided by Kresse and Hafner.[16] The valence electrons include the ones in the 3d and 4s orbitals of Cu, 4d, 5s, and 5p of In, and 2s and 2p of O.

In our study of point defects, the supercell approach was employed, in which a defect (α) is placed in an artificially large $CuInO_2$ supercell that is repeating itself in 3D space periodically. The shortest distance between defect and its image in the neighboring supercell equals the dimension of the supercell. Because of the noncubic structure of $CuInO_2$, its dipole and quadrupole correction[17] could not be calculated accurately. Thus, the dimension has to be large enough to eliminate dipole and quadrupole interactions between the defects. Monopole corrections were read from the output files of VASP.

Artificial supercells were constructed by repeating the fully relaxed conventional cell along the *a*- and *b*-axes, not the extraordinarily lengthy *c* axis, because its purpose is to avoid the artificial interaction between defects due to insufficient cell size. The effect of supercell size on defect formation energy was examined with a supercell size convergence test. Taking both the size convergence test and the computation cost into account, we employed the $3 \times 3 \times 1$ supercell with 108 atoms in the following work. Defect structures were relaxed with a mode that ions within a certain range (relaxation range) were relaxed, while the other ion positions, supercell size, and shape were fixed. The relaxation range was also carefully examined for each defect position.

3.2. Perfect Structure. In this section, we first apply VASP to the study of perfect $CuInO_2$ for its bulk properties and the structural parameters of the conventional cell. Supercells for the following point defect study were constructed from the perfect conventional cell. Then the electronic band structure and DOS of the material were calculated, which are the background of the defect levels.

The structure of $CuInO_2$ (*R*-3*M*) is composed of O−Cu−O dumbbell layers alternatively separated by the In monoatom layers. We have calculated the properties of $CuInO_2$ using a planewave cutoff energy of 500 eV and Γ centered grid $5 \times 5 \times 2$ k point sampling in the irreducible Brillouin zone (IBZ). The values resulted in convergence in the total energy to ≤1 meV per atom. Then the $CuInO_2$ primary cell was relaxed through geometry optimization with cell shape and ions relaxed while cell volume was fixed on about 30 sets of selected volumes. The results of the relaxed cells are fitted to the Murnaghan equation of state (EOS)[18] to find the ground state lattice constants. The lattice parameters of the fully relaxed structure were found to be $a = 3.356$ (3.292) Å and $c = 17.531$ (17.388) Å, with the experimental values[1b] in parentheses.

The electronic band structure was calculated on a $CuInO_2$ unit cell containing four atoms. From the electronic band structure, it was found that the minimum value of the conduction band is located at the Γ point, while the maximum value of the valence bands is at the F point. Thus, $CuInO_2$ has an indirect band gap of about 0.32 eV. The lowest direct band gap is at Γ of 0.68 eV.

(13) Kresse, G.; Furthmüller, J. *Comput. Mater. Sci.* **1996**, *6*, 15. Kresse, G.; Furthmüller, J. *Phys. Rev. B* **1996**, *54*, 11169.
(14) Perdew, J. P. In *Electronic structure of solids '91*; Ziesche, P., Eschrig, H., Ed.; Akademie-Verlag: Berlin, 1991. Perdew, J.; Wang, Y. *Phys. Rev. B* **1986**, *33*, 8800. Perdew, J.; Zunger, A. *Phys. Rev. B* **1981**, *23*, 8054.
(15) Vanderbilt, D. *Phys. Rev. B* **1990**, *41*, 7892.
(16) Kresse, G.; Hafner, J. *J. Phys.: Condens. Matter* **1994**, *6*, 8245.
(17) Makov, G.; Payne, M. C. *Phys. Rev. B* **1995**, *51*, 4014. Neugebauer, J.; Scheffler, M. *Phys. Rev. B* **1992**, *46*, 16067.
(18) Murnaghan, F. D. *Proc. Natl. Acad. Sci. U.S.A.* **1994**, *30*, 244.

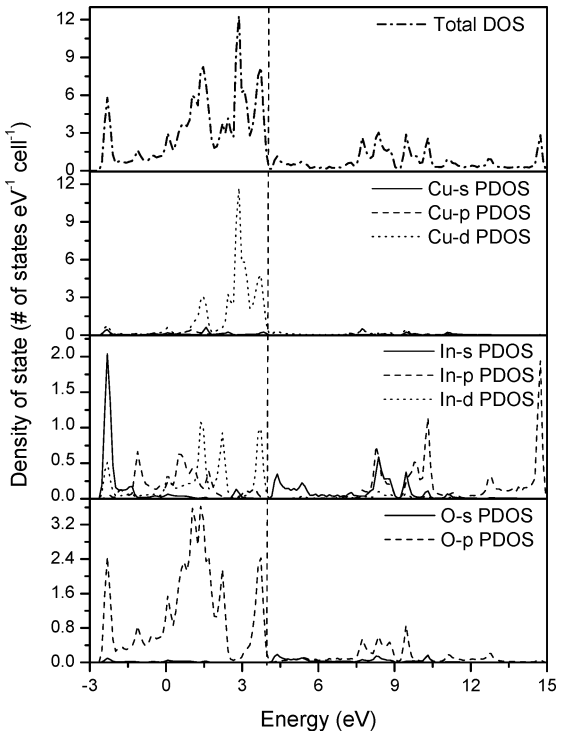

Figure 1. DOS and PDOS of $CuInO_2$ within GGA. The straight dash line crossing the whole figure indicates the VBM of $CuInO_2$. The top panel shows the total DOS of the material. Others show the PDOS of the s, p, or d orbital in the three component elements.

The total DOS and site- and angular-momentum projected DOS (PDOS) of $CuInO_2$ are plotted in Figure 1, where the origin of states in DOS could be found through analysis of each component's PDOS. There is a broad mass of valence band from −2 to 4 eV (that is the VBM). They are mainly derived from Cu d and O p states. The upper valence band is mainly from Cu d and O p states, with some Cu s and In d states involved. The O 2s states form a lower valence band at −17 eV from VBM (not shown). The lower conduction band near CBM is mainly composed of Cu d, In s, and O s states. A broader mass of conduction band is shown about 3 eV higher from CBM.

3.3. Isolated Intrinsic Point Defects. After determining the computational parameters in sections 2 and 3.1, our results on all intrinsic point defects in $CuInO_2$ are presented in this section. Twelve types of intrinsic point defects (see Table 1) were studied, including three interstitial, three vacancy, and six antisite species. Starting from the study of neutral intrinsic point defects in section 3.3.1, we obtained their formation energy and examined the dependence of defect formation energy on the chemical environment. Then in 3.3.2, several selective defect species (see Table 2) with reasonable formation energy at their neutral states were examined for all possible charge states. We show the dependence of the formation energy and the abundance of the defects on both the chemical environment and the doping conditions (E_F). In section 3.3.3, defect transition levels were then obtained. Intrinsic point defects were thus examined in terms of their effects on the electronic properties of $CuInO_2$ as shallow/deep donor/acceptor levels. It is noted that an antisite A_B means A occupying the B site. Whenever applicable, a numbered superscript indicates the defect charge that will be further explained in section 3.3.2.

Table 1. Formation Energy $\Delta H_f(\alpha,q=0)$ (eq 1) of All the Neutral Intrinsic Point Defects in Different Chemical Environments[a]

	formation energy of defect $\Delta H_f(\alpha,q=0)$/eV			
Cu-related defects	μ_{Cu} minimum	BG correction	μ_{Cu} maximum	BG correction
V_{Cu}	0.498	0.498	1.167	1.167
Cu_i	2.081	2.791	1.412	2.122
Cu_{In}	−0.391	−0.391	0.946	0.946
Cu_O	7.327	9.457	5.322	7.452
	formation energy of defect $\Delta H_f(\alpha,q=0)$/eV			
In-related defects	μ_{In} minimum	BG correction	μ_{In} maximum	BG correction
V_{In}	1.257	1.257	3.263	3.263
In_i	5.321	7.451	3.315	5.445
In_{Cu}	3.241	4.661	1.903	3.323
In_O	14.074	17.624	10.731	14.281
	formation energy of defect $\Delta H_f(\alpha,q=0)$/eV			
O-related defects	μ_O maximum	BG correction	μ_O minimum	BG correction
V_O	3.444	4.864	2.107	3.527
O_i	0.137	0.137	1.474	1.474
O_{Cu}	2.583	2.583	4.589	4.589
O_{In}	4.232	4.232	7.575	7.575

[a] Values after band gap corrections are given in "BG correction" column.

Table 2. Defect Formation Energies in Terms of $\Delta E(\alpha,q)$ (eq 4) and Defect Transition Levels $\epsilon_\alpha(q/q')$ (eq 5)

defect α	$\Delta E(\alpha,q)$/eV	n_{Cu}	n_{In}	n_O	q
Defect Transition Level: $(0/+1) = E_C - 1.11$ eV					
Cu_i^{+1}	2.55	+1	0	0	+1
Cu_i^{0}	2.83				0
Defect Transition Level: $(-2/-1) = E_V + 1.50$ eV; $(-1/0) = E_V + 0.39$ eV					
Cu_{In}^{0}	3.06	+1	−1	0	0
Cu_{In}^{-1}	3.46				−1
Cu_{In}^{-2}	4.96				−2
Defect Transition Level: $(-2/-1) = E_V + 1.50$ eV; $(-1/0) = E_V + 0.33$ eV					
V_{Cu}^{0}	1.17	−1	0	0	0
V_{Cu}^{-1}	1.50				−1
V_{Cu}^{-2}	3.00				−2
Defect Transition Level: $(-2/-1) = E_V + 1.77$ eV; $(-1/0) = E_V + 0.65$ eV					
O_i^{0}	0.14	0	0	+1	0
O_i^{-1}	0.79				−1
O_i^{-2}	2.56				−2
Defect Transition Level: $(-2/-1) = E_V + 1.31$ eV; $(-1/0) = E_V + 0.15$ eV					
V_{In}^{0}	5.38	0	−1	0	0
V_{In}^{-1}	5.53				−1
V_{In}^{-2}	6.85				−2
V_{In}^{-3}	9.27				−3
Defect Transition Level: $(0/+1) = E_C - 1.26$ eV					
V_O^{+2}	5.78	0	0	−1	+2
V_O^{+1}	4.74				+1
V_O^{0}	4.86				0
Defect Transition Level: $(0/+1) = E_C - 0.57$ eV					
In_i^{+3}	5.26	0	+1	0	+3
In_i^{+2}	3.05				+2
In_i^{+1}	2.51				+1
In_i^{0}	3.33				0
Defect Transition Level: $(0/+1) = E_C - 1.01$ eV					
In_{Cu}^{+2}	1.58	−1	+1	0	+2
In_{Cu}^{+1}	0.83				+1
In_{Cu}^{0}	1.58				0

3.3.1. Neutral Intrinsic Point Defects. On the basis of the supercell size analysis,[19] a 3 × 3 × 1 superimposing of the ground-state primitive cell was employed in all defect

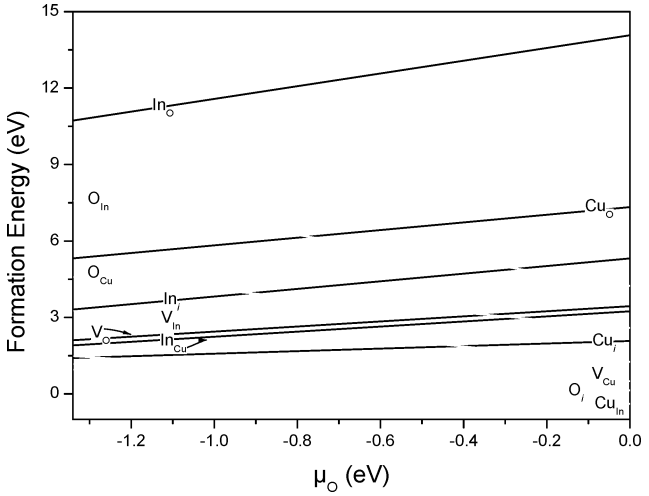

Figure 2. Chemical environment dependence of defect formation energies for all the neutral intrinsic point defects. Grey lines represent acceptor-like defects, whereas black lines represent donor-like defects.

calculations. A cutoff energy of 400 eV was employed in all the defect calculations. In addition, because of the large size of the $3 \times 3 \times 1$ supercell, only one *k* point is necessary to be considered for *k* space integrations.

Using the formalism discussed in section 2.1, the formation energy of the neutral intrinsic point defects in $CuInO_2$ was calculated. These defects include vacancies and interstitials of the three components, and the antisites of every component substituting each of the other two. All the neutral intrinsic point defects considered in this study and their formation energies are listed in Table 1, where 12 intrinsic neutral point defect types are grouped according to their related component type. The formation energy of each defect is given at the chemical potential limits of the related component. As antisite is actually associated with two components, they are grouped by the one substituting the lattice site to avoid repeat; e.g., Cu_{In} is listed in the Cu group.

Figure 2 shows the dependence of defect formation energy on the chemical potential of oxygen. For example, the lowest formation energy of O_i forms in oxygen-rich conditions ($\mu_O = 0$ eV) with $\Delta H_f(O_i) = 0.137$ eV, whereas it has the highest formation energy in oxygen-poor conditions ($\mu_O = -1.34$ eV) with $\Delta H_f(O_i) = 1.474$ eV. From Figure 2, we can see that donor-like defects have lower formation energy, i.e., they are easier to form, in oxygen-poor conditions, whereas acceptor-like defects are easier to form in oxygen-rich conditions. For example, the formation of V_{In} (acceptor-like) is easier in oxygen-rich conditions, but becomes difficult in oxygen-poor conditions, which is quite the opposite for V_O (donor-like). However, the formation of V_{Cu} (acceptor-like) is easier than that of both V_{In} and V_O, indicating the importance of oxygen and indium in constructing the crystal.

From Figure 2 and Table 1, we deduce that, independent of the partial pressure of oxygen, the most abundant intrinsic point defect in $CuInO_2$ is an acceptor-like defect, Cu_{In}. The next most abundant neutral intrinsic defect is O_i or V_{Cu}, depending on the partial pressure of O. Without intentional doping, $CuInO_2$ is abounding with acceptor-like intrinsic defects. This asymmetry in terms of intrinsic doping in $CuInO_2$ is also observed in $CuAlO_2$ and $CuGaO_2$.[4,5] The defects with lower formation energy at neutral states were also chosen for further study of charged defects and defect transition levels.

3.3.2. Charged Intrinsic Point Defects. Similar to the extrinsic point defects, intrinsic point defects can be predicted to be donor-like (donate electrons) or acceptor-like (accept electrons) simply by comparing the valence electrons of the defect and the host elements. Briefly, the charge states could be determined according to the defect type. For interstitials, the charge states are similar to the nominal valency that the element could be in its compounds, e.g. -2, -1, or 0 for O_i. For vacancies, defect states are created from the valence band states of the host. Thus, the charge states for V_O, for example, are 0, 1, and 2. For antisites, the charge states follow one of the above rules, depending on the relative valency of the intruder and the native. If the valency of the intruder is higher, it observes the rule for interstitial; otherwise, the rules for vacancies should be applied. For detailed discussions, refer to ref 20.

In our calculation, 8 of the 12 isolated intrinsic point defects, with relatively low formation energy in their neutral states, were chosen for charged defect study. As we are interested in the bipolar dopability, half of the candidates are donor-like defects and half are acceptor-like. On the basis of the methodology discussed in section 2.1, $\Delta E(\alpha,q)$ was calculated from eq 4 and the results are listed in Table 2. The defect formation energy $\Delta H_f(\alpha,q)$ at different chemical potentials and E_F can be deduced through eq 3. For example, for O_i^{-1} the lowest defect formation energy occurs in oxygen-rich conditions ($\mu_O = 0$) as E_F at the CBM ($E_F = 1.39$ eV) with $\Delta H_f(O_i^{-1}) = 0.79 - 0 + (-1) \times 1.39 = -0.60$ eV. Hence, the defect formation energy can be easily found by adding or subtracting the chemical potential and E_F values. The formation energy of donor-like defect is also subject to the band gap correction, as for neutral ones, which will be further discussed in section 4.2. In Table 2, transition levels within the electronic band gap or near the band edges are also listed, which will be discussed in the following subsection.

3.3.3. Defect Transition Levels. On the basis of the formalism discussed in section 2.1, the defect transition energy levels for different defect types with various charge states were calculated using the results listed in Table 2.

By varying E_F, we can simulate the effect of changes in dopant concentration. For dominant defects, the formation energies are shown in Figure 3 as a function of E_F at the two oxygen chemical potential limits. $\Delta H_f(\alpha,q)$ also varies as a function of doping level. The slopes of the lines in the figures correspond to the charge state of the defect. For each defect, the line for a particular charge state is shown over the range where this charge state has the lowest energy of all possible charge states. The kinks thus correspond to the transitions between charge states. For example, in oxygen-rich conditions (see Figure 3a), V_{Cu}^0 has the lowest formation energy of 0.498 eV when E_F is 0.33 eV above VBM ($E_F = 0$ eV). As E_F moves further toward the CBM, V_{Cu}^{-1} becomes the stable charge state. The formation energy of V_{Cu}^{-1}

(19) Liu, L. Master Thesis, National University of Singapore, Singapore, 2005.

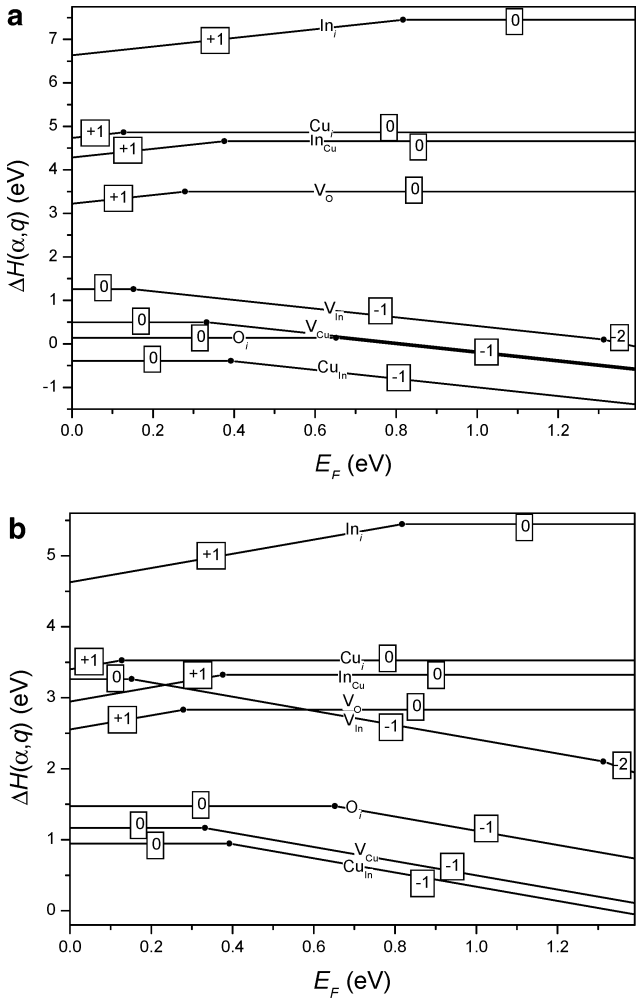

Figure 3. Formation energies of eight intrinsic defects as a function of E_F in (a) oxygen-rich conditions and (b) oxygen-poor conditions. Charge states q determine the slope of each line segment. Solid dots denote values of E_F where transition between charge states occur.

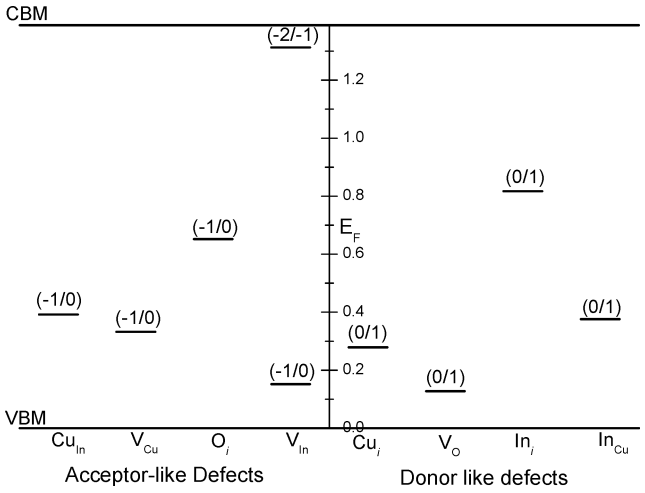

Figure 4. Defect transition levels of intrinsic point defect in $CuInO_2$. The left panel contains transition levels of acceptor-like defects that interact with VBM; the right panel shows donor-like defects related to the CBM. The numbers in parentheses denote the charge states of the transition level, e.g. (−1/0) indicates that the neutral state is stable below the transition level and −1 state becomes dominant as E_F moves toward the CBM.

linearly decreases at a rate equal to its charge state −1. The kink in the V_{Cu} line is its acceptor level or (−1/0) charge state transition level. From Figure 3, it is clear that Cu_{In} antisite has the lowest formation energy and thus the highest population for all E_F positions at both oxygen limiting chemical potentials.

4. Discussions

In this section, miscellaneous respects of our calculations are discussed, such as the effect of correction on the calculated band gap on the defect formation and defect levels and the relaxation of neighboring atoms around defects.

4.1. Effect of Intrinsic Defects on Electronic Properties. Figure 4 shows the defect levels in a more straightforward way. From Figure 4, we can see that V_{In} produces a shallow acceptor (−1/0) transition level at about 0.15 eV above the VBM. V_{Cu} and Cu_{In} provide relatively deep acceptor levels at 0.33 and 0.39 eV above the VBM, respectively. Although they produce slightly deeper charge transition levels than V_{In}, they are expected to be abundant due to their lower formation energies. On the other hand, the calculation results predict that donor-like intrinsic point defects in $CuInO_2$ form very deep transition levels. As a result, intrinsic point defects do not support active n-type conductivity. Moreover, defect formation energy values for these donor-like point defects are higher than 2.5 eV, which is very likely to suppress their formation under thermodynamic equilibrium conditions. This predicts the possible p-type conductivity in the defect structured $CuInO_2$. However, experimentally it is an insulator without intentional doping. The experimental result could be attributed to many different causes, including lack of target defects in the ionic-exchange fabrication process or mixing of other binary or ternary compounds that can compensate p-type conductivity. It is also noted that this work focuses on the thermodynamics of defect formation, whereas kinetic effects should be carefully considered in the actual design of the material and the interpretation of experimental results.

No experimental studies on the defect mechanism of $CuInO_2$ have been published yet; however, Ingram et al. studied the transportation and defect mechanism of $CuAlO_2$,[21] $CuScO_2$, and $CuYO_2$.[22] They suggested that the defect physics of $CuM^{III}O_2$ delafossite is directly related to the size of the M-site cation. As the size of In^{3+} is between those of Sc and Y, the experimental results of Sc and Y may enlighten the defect physics of $CuInO_2$. Slightly increased P_{O_2} (O_2 partial pressure) dependences of the conductivity of $CuMO_2$ (M= Sc or Y) were observed, which was suggested to indicate an important role played by the extra O_i for hole-doping, although not the dominant defect under the experimental conditions. Our results (see Figure 3) also suggest that O_i is not the dominant intrinsic defect in $CuInO_2$. However, P_{O_2} influences the hole-doping not through O_i but via a rather indirect way by decreasing the formation energy of V_{In} and other acceptor-like defects. Moreover, Ingram et al. indicated that no evidence suggests V_{Cu} as the dominant defects in the defect structures, whereas our calculations show

(20) Wei, S.-H.; Zhang, S. B. *Phys. Rev. B* **2002**, *66*, 155211.
(21) Ingram, B. J.; Mason, T. O.; Asahi, R.; et al. *Phys. Rev. B* **2001**, *64*, 155114.
(22) Ingram, B. J.; Harder, B. J.; Hrabe, N. W.; et al. *Chem. Mater.* **2004**, *16*, 5623.

that Cu_{In} antisite is the dominant intrinsic point defect, but V_{Cu} could be important in oxygen-poor conditions.

4.2. Band Gap Correction and Its Effect on Defect Levels. Due to the ground-state feature of the DFT method, calculated band gap values are generally underestimated, so that the calculated band gap has to be corrected. As proposed by Nie et al.[5] and further confirmed by our calculations, the measured optical band gap of $CuInO_2$ is the "apparent band gap", corresponding to the band edge difference at the L position in the IBZ. In a recent optical absorption study on $CuInO_2$, Teplin et al.[6] observed some optical absorption in 1−2 eV, below the optical band gap. This could be explained as the absorption at indirect band gap (as the authors did) or between defect levels. This could also result from the absorption, more interesting, at Γ, the minimum direct band gap, as the transition matrix elements are nonzero although low at Γ.[12] Hence, the LDA correction is calculated as 0.71 eV, the difference between the experimental band gap value (3.9 eV) and the calculated direct band gap at L (3.19 eV). Then the band gap is scissored in the middle and then sewn with the CBM shifting 0.71 eV upward. As the calculated minimum direct band gap is 0.68 eV at Γ, the value becomes 1.39 eV after band gap correction.

Consequently, we can expect that the defect (transition) levels in the gap need to be corrected accordingly. We assume that the acceptor-like defect levels will not be affected by the band gap correction, as they are related to the VBM. Formation energy of acceptor-like defects is also not subject to any band gap correction. Only the defect levels of the donor-like defects follow the CBM shift of the same amount. Meanwhile, defect formation energy was corrected accordingly. A crude way to do this is by increasing the formation energy values of the donor-like defects by $0.71n_{elect}$ eV, where n_{elect} is the number of valence electrons occupying the defect level; e.g., 2×0.71 eV, 1×0.71 eV, and 0×0.71 eV were added to the formation energy of V_O at 0, +1, and +2 charge states, respectively.

Now, let us see the effect of band gap correction on our previous conclusions about defect transition levels. As mentioned above, both the formation energy and the defect transition levels of the acceptor-like defects are not affected by the band gap correction. Hence, we only need to examine the effect of correction on donor-like defects. This will be discussed in two respects: defect levels and defect abundance.[11]

Instead of the absolute values in the band gap, we are interested in the relative positions of the defect levels to their related band edges, e.g., the CBM for donor-like defects. As the donor-like defect levels shift the same amount as the CBM, our conclusions about them as deep or shallow levels do not change with or without band gap corrections.

Band gap correction cannot vary our conclusions on the relative abundance of intrinsic defects, either. In oxygen-rich conditions, the most abundant four defects, as can be seen in Table 1, are Cu_{In}, V_{Cu}, O_i, and Cu_i before band gap correction; after band gap corrections, the first three defect types, all acceptor-like, still dominate in oxygen-rich conditions. In oxygen-poor conditions, the formation energy of donor-like defects decreases, especially for Cu_i. But their formation energy is still higher than p-type defects Cu_{In} and V_{Cu} before band gap correction; those two p-type defect species still dominate after band gap correction. Furthermore, as Cu_i is a deep donor-like defect, its formation does not contribute much to the conductivity. Thus, the relative abundance of the intrinsic point defects does not change after the band gap correction.

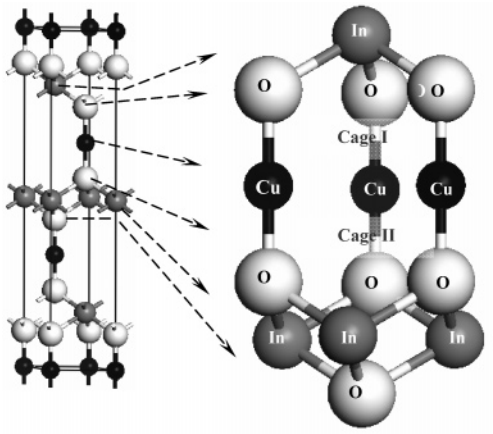

Figure 5. Schematic drawing of cage I (O_3Cu_3) and cage II (Cu_3O_3) for interstitial sites; the two cages are a bit different at the far ends in terms of chemical environment. The small drawing on the left is the conventional cell of delafossite, showing position of the interstitial cages in a conventional cell.

Therefore, Cu_{In} and V_{Cu} are the most abundant intrinsic defects in both oxygen-rich and oxygen-poor conditions. Band gap corrections do not alter our conclusions on the defect levels or the relative abundance of intrinsic point defects. Acceptor-like intrinsic defects dominate in the nonintentionally doped material. Asymmetry in terms of intrinsic doping can be observed in $CuInO_2$ from our intrinsic point defect calculation.

4.3. Ionic Relaxation and Response toward External Pressures. The changes of the atom positions neighboring to different defect species were also examined. For interstitials, asymmetrical relaxation was observed. Both cage I and cage II (see Figure 5) are occupied by some ions based on the interstitials' signs of charge. Different from what was expected for O_i, the center of the Cu_3 triangle is not occupied by O_i in this work. Cation interstitials (Cu_i and In_i) were found to occupy cage II, close to the Cu_3 layer, probably due to the size effect (O^{2-} is huge compared with Cu^+). O_i is in cage I and is close to the Cu_3 layer. Different preference of interstitials for cage I or cage II confirms the different chemical and electronic environment in the two cages because of the difference in packing sequences adjacent to the two ends of the $O_3-Cu_3-O_3$ cage.

For vacancies and antisites, ions were found to relax in two different ways. Each shell of atoms around the defects at Cu or In positions relax symmetrically, whereas the atoms around the oxygen-position-related defects relax asymmetrically, mainly due to the asymmetrical chemical and structural environment around it. It is also interesting to compare the changes of neighboring positions for Cu and In vacancies, where both of them have symmetrical nearest neighbors with oxygen as the nearest neighbors, cations of the same kind as the next nearest neighbors, and cations of the other kind as the third nearest neighbors. When an In is removed from

a supercell, its nearest neighbors (O) move away from it due to the loss of bonding, whereas the neighbors (O) move toward V_{Cu} to reduce the open space.

Assuming atoms in a lattice are spherical with their size determined by the elements' ionic radii,[23] we may find the packing efficiency in the $[CuO_2]$ dumbbell layer and that of the $[InO_2]$ edge-sharing octahedral layer. The packing efficiency in the $[CuO_2]$ layer (32%) is found to be less than half of that in the $[InO_2]$ layer (80%). Hence, we may expect a much more compact $[InO_2]$ layer and a relatively roomy $[CuO_2]$ layer. Moreover, as the ionic radii of the three component elements are able to give a good approximation of the interatomic distances,[7] we have more confidence in the estimated packing efficiency. Because of the layered structure and the difference in packing efficiency in the alternate layers, oxygen atoms, at the interface of the layers, are very likely to have different dependence on its neighboring cations. The difference in packing efficiency also determines that the interstitials could be accommodated in one of the Cu_3-O_3 cages (Figure 5).

For interstitials, the size effect dominates while the electrostatic effect also influences the deformation of the lattice around an interstitial. An interesting phenomenon was observed in the oxygen interstitial case: Instead of being pushed aside from the interstitial site in the $a-b$ plane, as what happens in cation interstitial cases, the nearest Cu_3 neighbors are attracted to O_i, although they moved further away from O_i in the c-direction due to the size effect. Comparing the formation energy of O_i and Cu_i, we may find that O_i is easier to form than Cu_i, although Cu cation is much smaller. It is attributed to the electronic repulsion between Cu_i to the nearest Cu_3 cations.

The changes of lattice vectors a and c with respect to the external pressure were also examined (see Figure 6) after the geometry optimization. It can be seen that the magnitude of the lattice vector a increases much faster than that of c; the c/a value decreases as the external pressure increases. In other words, the a vector is easier to deform than the c vector. A similar response to the external compressing was observed in $CuFeO_2$,[24] $PtCoO_2$,[25] and $CuGaO_2$.[26] No report on the mechanical property of $CuInO_2$ is presented so far, as single-crystal $CuInO_2$ has proven difficult to make and has never been made. From this work, we may expect a similar response of $CuInO_2$ to the compressive pressure. We also extend our knowledge of delafossite's response toward external pressure from the compressive to expansive pressure conditions.

Point defects may introduce stress and strain in their neighborhood, so does the external pressure. The difference is that the former is microscopic while the latter is macroscopic. In this sense, the different responses of its neighbors toward the formation of each vacancy species may be related

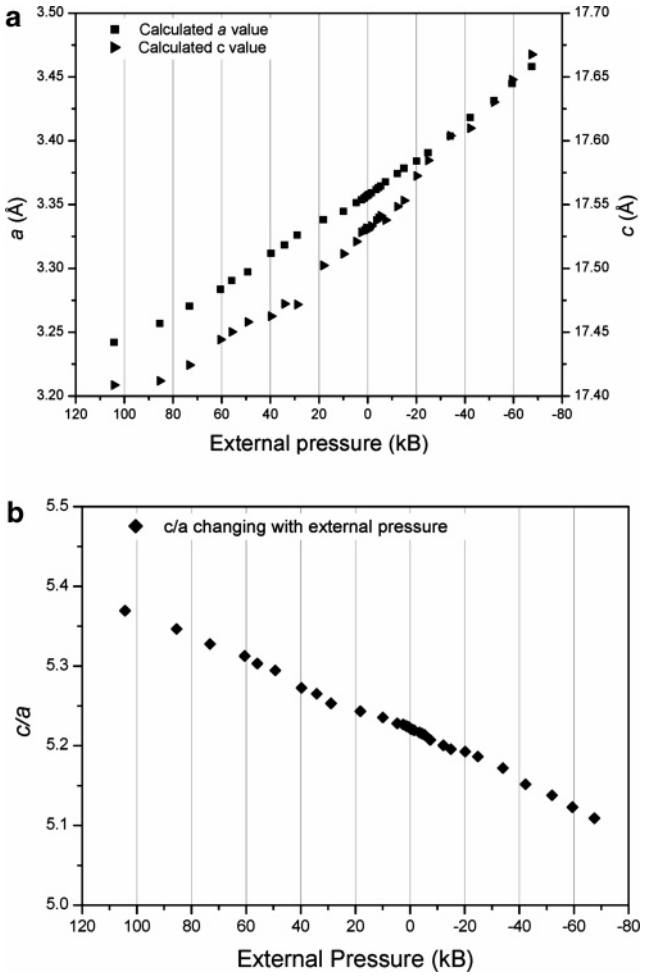

Figure 6. Dependence of (a) the magnitudes of the calculated lattice constants a and c and (b) the ratio c/a of $CuInO_2$ with external pressure. For external pressure values, a positive sign represents compressive pressure, while a negative sign is for expansive pressure.

to the macroscopic anisotropism toward the external pressure. For a layered structure as delafossites, anisotropism is readily expected, like that of graphite. However, with chemically different layers in the ternary compound, there could be different causes for the anisotropic property. Actually, the vibration of packing efficiency from layer to layer may have great influence on the anisotropic deformation. With the relatively compact packing in $[InO_2]$ layers, the lattice is less capable of deforming in the $a-b$ plane, whereas in the c-axis, the lattice could be expand or contract without too much energetic compensation due to the roomy $[CuO_2]$ layers. Therefore, the mechanical anisotropism in $CuInO_2$ is caused not only by the difference between interlayer and in-layer forces as in graphite but also the different packing efficiency and the bonding strength between different species of atoms.

5. Conclusions

Theoretical calculations on isolated point defects in $CuInO_2$ were carried out to find their formation energies and defect transition levels. The problem was approached by using a plane-wave basis set, a pseudopotential technique, and the supercell method.

As a systematic study on the intrinsic point defects in $CuInO_2$, 12 neutral intrinsic point defects, all possibilities

(23) Shannon, R. D. *Acta Crystallogr. A* **1976**, *32*, 751. Shannon, R. D.; Prewitt, C. T. *Acta Crystallogr. B* **1969**, *25*, 925.
(24) Zhao, T. R.; Hasegawa, M.; Kondo, T.; et al. *Mater. Res. Bull.* **1997**, *32*, 151.
(25) Hasegawa, M.; Tanaka, M.; Yagi, T.; et al. *Solid State Commun.* **2003**, *128*, 303.
(26) Pellicer-Porres, J.; Segura, A.; Ferrer-Roca, Ch.; et al. *Phys. Rev. B* **2004**, *69*, 024109.

for a ternary compounds, were examined. Eight of them with reasonably low formation energy at the relevant neutral states were examined for their charged states. Our results show that acceptor-like intrinsic point defects generally have lower formation energies. We may expect p-type intrinsic defects being outnumbered in $CuInO_2$ without intentional doping. Moreover, some p-type intrinsic point defects have shallow defect-transition levels in the band gap, whereas most donor-like intrinsic defects form deep defect levels. There is intrinsic doping asymmetry in terms of n- vs p-type defects in $CuInO_2$. High formation energy combining deep defect transition levels with donor-like intrinsic defects make $CuInO_2$ unlikely to have n-type conductivity without intentionally doping. On the other hand, low formation energy and shallow defect levels for p-type intrinsic defects may bring p-type conductivity for $CuInO_2$ with intrinsic defect structure, which might be suppressed by the formation of a secondary phase, like In_2O_3 in the experiment.

Acknowledgment. This work as sponsored by the Agency of Science, Technology and Research of Singapore (A*STAR). We wish to thank Dr. Michael Sullivan for reading the manuscript.

CM051048K